






Article

The Use of SAR Offset Tracking for Detecting Sand Dune Movement in Sudan

Ahmed Mutasim Abdalla Mahmoud ^{1,2,*}, Alessandro Novellino ², Ekbal Hussain ²,
Stuart Marsh ¹, Panagiotis Psimoulis ¹ and Martin Smith ^{1,†}

¹ Nottingham Geospatial Institute, University of Nottingham, Nottingham NG7 2TU, UK; Stuart.Marsh@nottingham.ac.uk (S.M.); panagiotis.psimoulis@nottingham.ac.uk (P.P.); martin.smith@nottingham.ac.uk (M.S.)

² British Geological Survey, Environmental Science Centre, Keyworth, Nottingham NG12 5GG, UK; alessn@bgs.ac.uk (A.N.); ekhuss@bgs.ac.uk (E.H.)

* Correspondence: ahmed.mahmoud@nottingham.ac.uk

† Retired.

Received: 14 September 2020; Accepted: 15 October 2020; Published: 17 October 2020



Abstract: Sand movement is one of the main environmental hazards in Northern Sudan that threaten livelihood and rural communities. This paper investigates for the first time the use of the Synthetic Aperture Radar (SAR) offset tracking technique for detecting sand movement in Northern Sudan, and distinguishes the impact of the movement influencing factors: wind speed/direction, vegetation and topography. High-resolution images from the Sentinel-1 satellite were used for the generation of displacement maps. Three different dune fields with different characteristics were investigated for a study period between 4 June and 14 October 2017 (133 days). Dune field 1 is vegetated and near a built-up area, dune field 2 is in an open environment with sand dunes overlaying rocky substrate, and dune field 3 is located near mountains. The cumulative east displacement over the study period was 1.8 m, −1.1 m and 4.8 m for the three dune fields, respectively, while the cumulative north displacement was 0.7 m, 2.9 m and 4.2 m. Large movement is detected in the non-vegetated dune fields, with an average dune velocity of 0.18 m/d, while the vegetated dune field had a velocity of 0.09 m/d, which emphasizes the fact that vegetation is an effective stabiliser of dune movement. The pixel offset results showed a positive correlation between the wind speed/direction and the dune movement. In addition to vegetation, topography also played a major role in diverting the direction of the blown sand mainly near the edges to the mountains and the vegetation barriers. This technique showed high competency in monitoring the movement of sand dunes, in addition to identifying areas exposed to large sand drifting as a risk mapping technique.

Keywords: Sudan; sand movement; sand dune detection; SAR; offset tracking; pixel offset

1. Introduction

Sand movement is one of the main environmental phenomena in Sudan that threaten livelihood and rural communities, where sand overwhelms built-up areas, agricultural fields, and irrigation canals [1–3]. Moreover, it affects the River Nile by shaping its banks [1,4]. Several factors influence the movement of sand: (i) the variation in near-surface wind direction and speed, (ii) the grain size and the characteristics of dune sands, which determines the size and spacing of dunes [4], and (iii) the vegetation coverage [5].

Sand dunes can move very rapidly, which presents a challenge for monitoring [6]. Due to the large area of desert in Sudan, traditional land surveying techniques (e.g., GNSS, levelling) are not effective for monitoring dune field motions because of the size of the areas to be investigated and the

costs involved. However, these techniques can be used to measure the elevation changes of individual dunes by repeating surveys [7].

Synthetic Aperture Radar (SAR) data captured from satellite sensors are widely used for earth observation [8], where it has been applied for monitoring the changes of forests canopy [9], detecting land subsidence [10], modelling the deformation of earthquakes [11], volcanoes [12], landslides [8,13] and floods [14]. SAR data have also been used for modelling sand dunes, where several case studies were conducted using the interferometric synthetic aperture radar (InSAR) technique for mapping desert dunes [15], in particular for the estimation of their volume [16] and height [17] of dunes. Additionally, coherence maps generated by InSAR are used to analyse the dynamics of sand dunes [18]. However, the InSAR technique struggles to measure rapid dune motions due to the loss in coherence between repeat SAR acquisitions.

In this study, the use of SAR offset tracking technique was investigated for detecting the movement of sand dunes. This technique determines the offset between pixels of the same area that appear in two different SAR images. The accuracy of offset tracking depends on the pixel size of the SAR images [13], and it is about 1/30th of the image pixel size for both range and azimuth directions [19], which results from errors in the co-registration of the two images [20]. In the case of Sentinel 1, this is 0.3 m. The main advantage of using offset tracking over Interferometric SAR (InSAR) is that it performs better at estimating large displacements beyond the maximum detectable deformation [21], and also where coherence is low [22], while avoiding the error-prone unwrapping step used in InSAR for the generation of velocity maps [20]. Finally, offset tracking can detect the movement in both range and azimuth directions which can be used to compute the horizontal displacement vectors [20]. Offset tracking techniques have been applied widely for studying glacier motion in Monacobreen [22] and in Argentina [20], for the estimation of landslides [13,23,24], and the deformation monitoring of earthquakes [23,24], deformation of coal mines [25] and volcanoes [19].

Pixel offset was used before for the detection of dune motion on Mars applied on optical images [26]; however, this is the first study that applies offset tracking on SAR images for detecting sand dune movement. In this paper, we measure the magnitude and direction of movement of sand dunes over three dune fields in Northern Sudan. We investigate the impact of the topography, vegetation cover and wind behaviour (speed and direction) on dune movement by using SAR images with small temporal baselines (12 days) of the SAR images to reduce decorrelation effects.

2. Study Area

Northern Sudan is the most affected region for sand dune movement in Sudan [1]. Epigraphic evidence found in the temple of Taharqo at the Kawa archaeological site in Northern Sudan records an inscription of Irike-Amanote, a Kushite King of Meroe, showing the clearing of sand from the processional way in the second half of the 5th century BC [1]. This means that sand movement is an ancient environmental phenomenon in Sudan. More recently, this issue has been exacerbated by the increasing aridity and spread of the Sahara Desert due to climate change [27].

The region of interest for this study covers an area approximately 75 km × 75 km in Northern Sudan within the Nubian Desert (Figure 1), where sand dunes are the dominant type of land cover. We investigated dune motions in three distinct dune fields within the study area. Dune field 1 is in a built-up area near to houses on the east bank of the River Nile at Golied city. In this area, locals use vegetation, such as *Prosopis juliflora* (mesquite) and *acacia mellifera* (kitr), to stabilize sand from overwhelming their crops and houses [1]. Dune field 2 is a field with dominant land cover of sand dunes where individual dunes can be identified from the rest of land cover, which consists of barren land and small rocks and it is also surrounded by small mountains on the eastern side. The dunes have approximate dimensions of 120 metres wide, 150 metres long and 20 metres high. Dune field 3 lies in a mountainous area and is bounded by small mountains on the eastern and western sides (Figure 2).

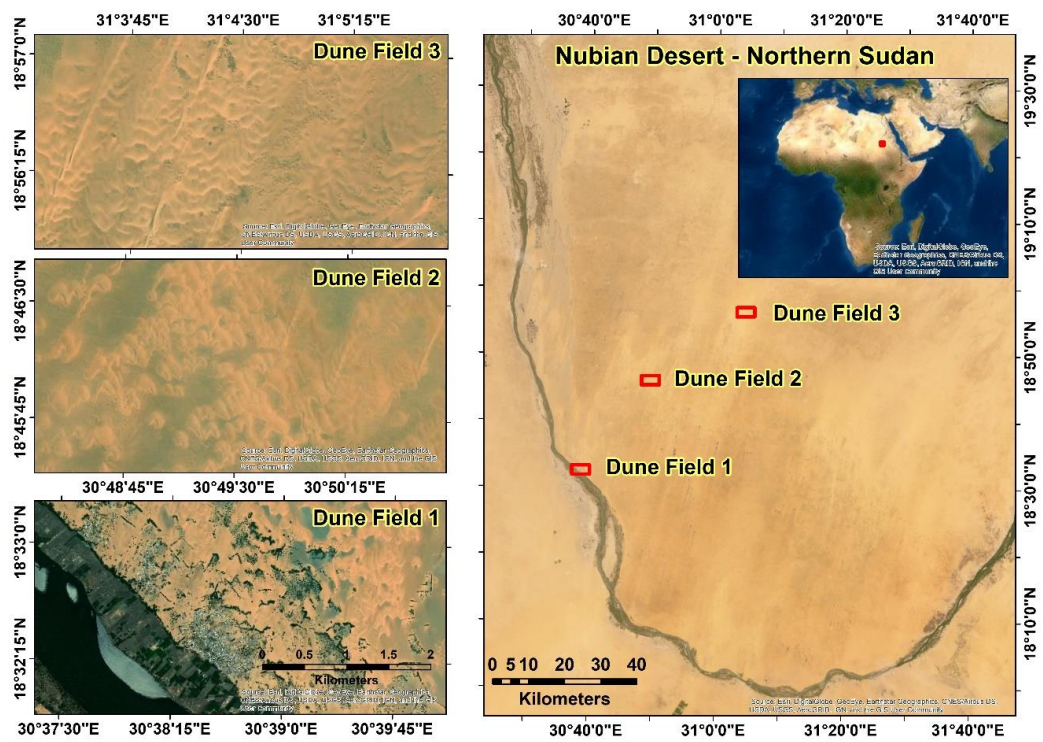


Figure 1. Study area in the Nubian Desert, Northern Sudan, with the three dune fields of interest; Dune field 1 is affected by vegetation, Dune fields 2 and 3 both have no vegetation. (Background image © Sources: Esri, DigitalGlobe, GeoEye, i-cubed, USDA FSA, US.)

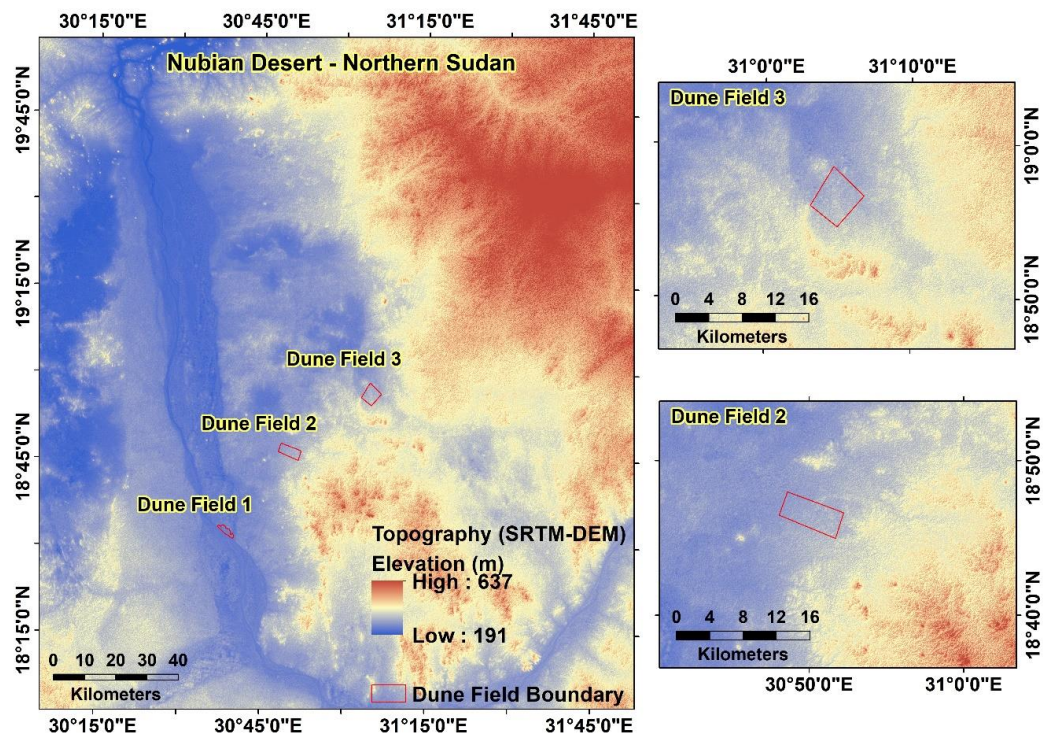


Figure 2. The topography of the study area.

3. Materials and Methods

3.1. Materials

3.1.1. SAR Images

Ten Sentinel-1 Level-1 Ground Range Detected (GRD) VV/VH polarised SAR images were used for offset tracking to determine the displacement of sand dunes in the study area for a period of five months encompassing a large sand storm that hit Northern Sudan on 12 August 2017 [28]. The GRD images have pixel spacing of 10×10 m and combined to form nine pairs for the dates between 4 June and 14 October 2017 (Table 1). The frequency of the Sentinel-1 acquisitions is 12 days at this latitude. We used GRD instead of single look complex (SLC) data because the pixel offset technique available in SNAP works on GRD products and only requires the amplitude information and not the phase. Additionally, the GRD products are already projected to ground range using an Earth ellipsoid model, which reduces the processing time.

Table 1. Image pairs used to generate displacement maps for the study area.

Image Pairs	Primary Image	Secondary Image
Image Pair 1	4 June 2017	16 June 2017
Image Pair 2	16 June 2017	10 July 2017
Image Pair 3	10 July 2017	22 July 2017
Image Pair 4	22 July 2017	3 August 2017
Image Pair 5	3 August 2017	15 August 2017
Image Pair 6	15 August 2017	8 September 2017
Image Pair 7	8 September 2017	20 September 2017
Image Pair 8	20 September 2017	2 October 2017
Image Pair 9	2 October 2017	14 October 2017

3.1.2. Wind Data

The European Centre for Medium-Range Weather Forecast (ECMWF) provides vector wind data for the globe [29,30]. ERA5 is the fifth generation of ECMWF reanalysis data generated by the Copernicus Climate Change Service Information, modelled using archived data from 1950 onwards. This is calculated using a climate–atmosphere model and data assimilation system named Integrated Forecasting system-based 4D-Var, which provides hourly estimates of atmosphere quantities [31]. For this study we used the U (east) and V (north) wind components, in the units of ms^{-1} , from the ERA5 model provided on an hourly basis at a height of 10 metres above the surface at 0.25° grid resolution. Please note that the wind data resolution is coarse compared to the individual dunes within a dune field. We assume that most of the sand motion was caused by winds near the surface of the sand. U and V wind components were combined to compute the horizontal wind speed and wind direction for the period June–October 2017 (Figure 3).

It should be noted that the ERA5 data is a reanalysis product and does not take into account the local high-resolution topography and potential vegetation, trees, etc. [31], which have a significant impact on the local wind speed and direction, and the movement of the dunes.

During the study period, the U wind component varies between east and west, but predominantly blows from the east, while the V component mostly blows from the south with considerable variation motion from the north.

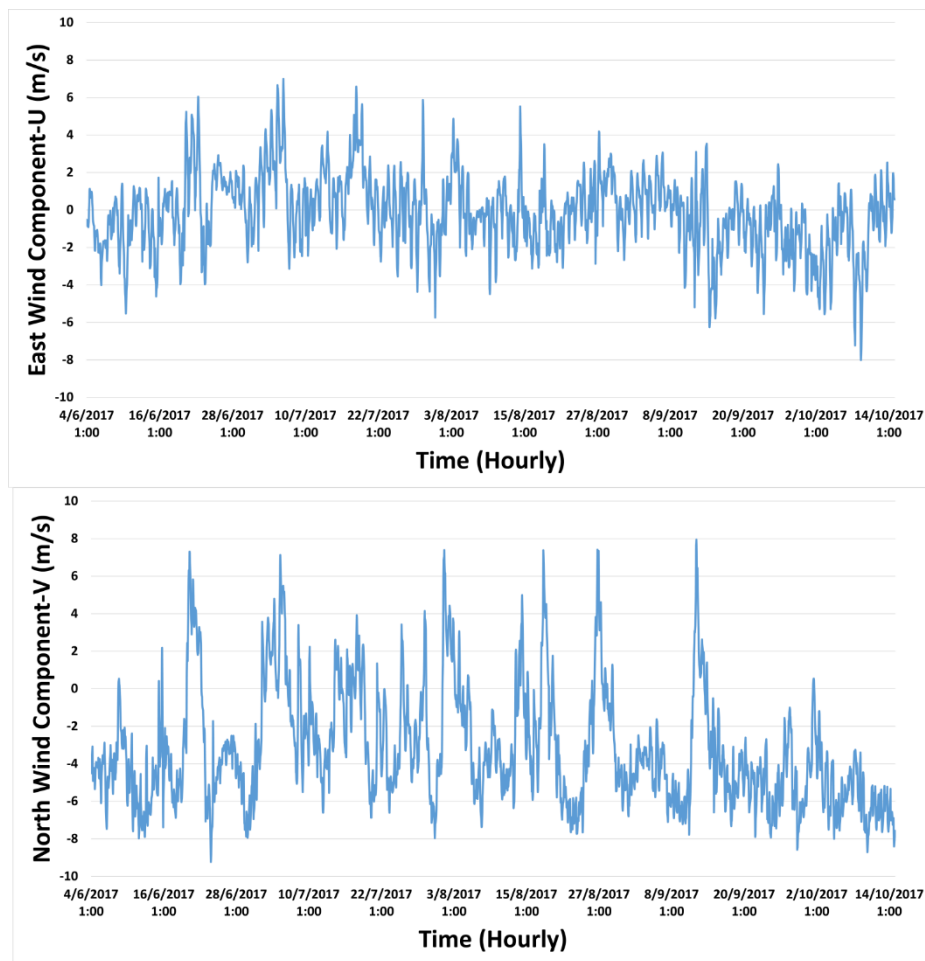


Figure 3. East and north wind components between the 4th of June and the 14th of October 2017.

3.2. SAR Pixel Offset Method

Sentinel-1 GRD images were processed using the Sentinel Application Platform (SNAP) provided by the European Space Agency (ESA) and available at <http://step.esa.int>. This toolbox provides a package of tools for SAR imagery processing including pixel offset tracking. The Sentinel-1 GRD data first need to undergo a pre-processing step before pixel offset tracking can be applied. First precise orbit files that contain the information of the location of the satellite at the time of acquiring SAR images were used to co-register each individual pairs and align the pixels between the secondary image and the primary image to within a few tenths of a pixel in range and thousandths of a pixel in azimuth. To reduce processing time a crop around the study region was taken from the co-registered dataset. Offset tracking is implemented in several sub steps. The pixel offset steps work on computing secondary ground control points (GCPs) that correspond to the user specified GCP grid on the primary image using normalized cross correlation. Then, the offset and the movement velocity between the primary and secondary GCPs positions are computed. The computed velocities of points are compared to the maximum velocity, with the latter defined based on previous studies in the same study area where the observed sand drift rate was $4.53 \text{ (m}^3 \text{ per linear metre width per year)}$ observed by sand traps [1]; therefore, we used a maximum velocity of 5 m/day to ensure observing all the movement of the dunes on short temporal period (days). Points with larger values are considered outliers. A local average is applied to valid GCPs. Figure 4 illustrates the steps of generating velocity maps using SNAP. Table 2 shows the offset tracking parameters used to generate the velocity maps.

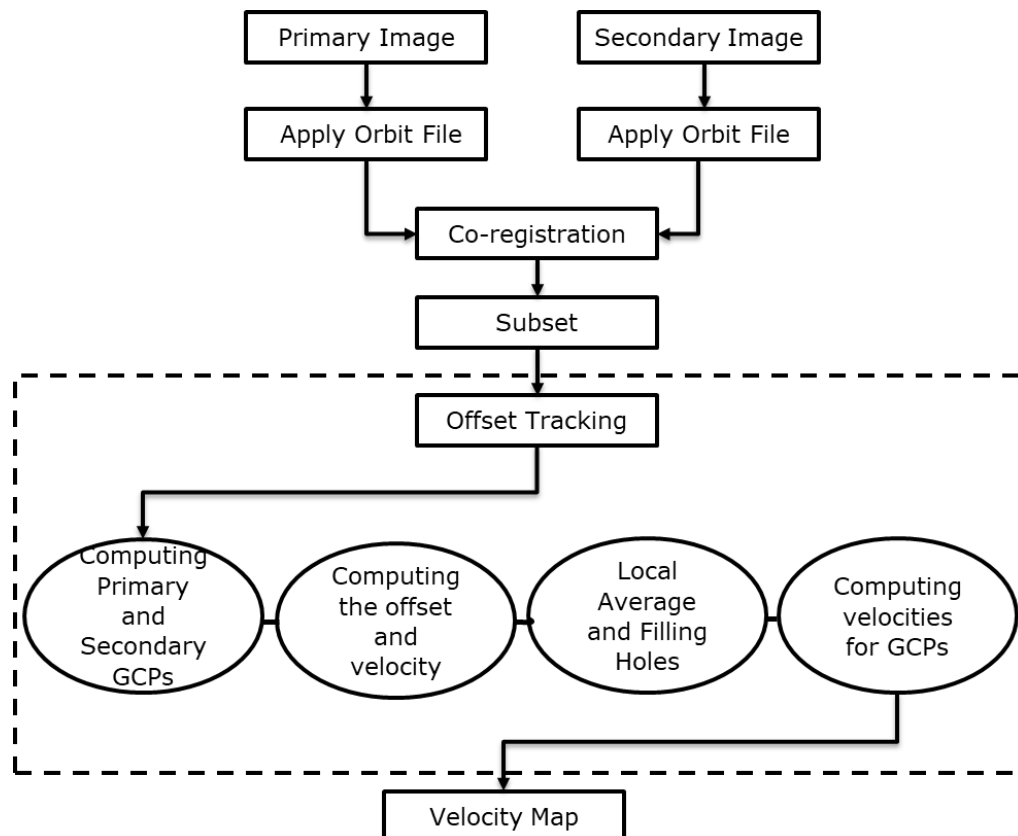


Figure 4. The steps of generating velocity maps using SNAP.

Table 2. Offset tracking parameters.

Parameter	Values
Grid Range and Azimuth Spacing (in meters)	400 × 400
Total GCP Points	31,648
Registration Window Width and Height	128 × 128
Cross-Correlation Threshold	0.1
Average Box Size	5
Max Velocity (m/d)	5.0
Radius for Hole Filling	4

A file that contains vector points of the grid GCPs velocities was also generated after applying offset tracking. This file contains the GCPs coordinates, displacement, velocity, heading (direction of movement), azimuth shift and slant range shift. These parameters were used to characterise the movement of the dunes.

A sequence of displacement vector maps for the study area were generated to study the dunes movement and relate these movement to influencing factors. By daisy chaining the image pairs, we were able to estimate the displacement time series for each pixel.

Since buildings are generally not built on moving sand dunes, we assumed that points over built up areas remain stable and are not displaced by the wind. This allowed us to define a threshold of motion to define a ‘stable’ displacement threshold. Any displacements beyond this level can be attributed to wind-driven motion.

Therefore, we first selected pixels over buildings and calculated the mean displacement and standard deviation for each image pair (Table 3). The average displacement (0.62 ± 0.46 m) for the studied period was used to distinguish between small and large displacements of sand dunes. Figure 5 illustrates part of the built-up areas and GCPs that fall within it.

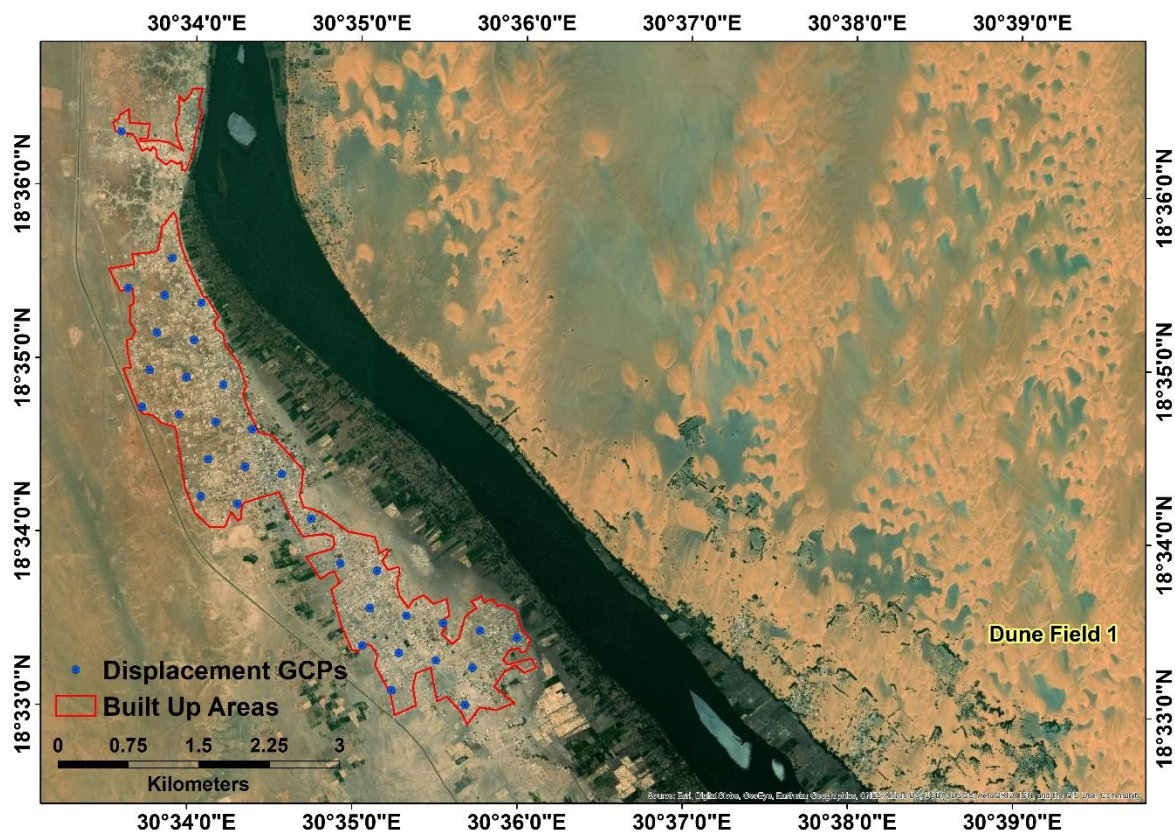


Figure 5. Displacement GCPs that fall within built up areas with an average displacement of 0.62 m.

4. Results

4.1. Displacement of Sand Dunes

On average, the measured dune displacement in each of the nine offset image pairs was about 0.7 m, 2.4 m and 2.6 m in dune fields 1, 2 and 3, respectively (Figure S1), where the three dune fields contained, respectively, 52, 49 and 81 dune points. However, there is considerable variation between the images. In a single offset image, the average dune displacement varies between 0.4 and 1 m in dune field 1, 1.3 and 3.5 m in dune field 2, and 1.8 and 3.8 m in dune field 3. Since offset images were created using consecutive SAR dates, we can temporally combine the offsets from each pair into a displacement time series. The east and north displacements for every GCPs in each dune field were averaged (Figure S2) to give the spatially averaged displacement time series for each dune field (Figure 6). The cumulative east displacement over the four months study period was 1.8 m, -1.1 m and 4.8 m for dune fields 1, 2 and 3, respectively, while the cumulative north displacement was 0.7 m, 2.9 m and 4.2 m (Figure 6).

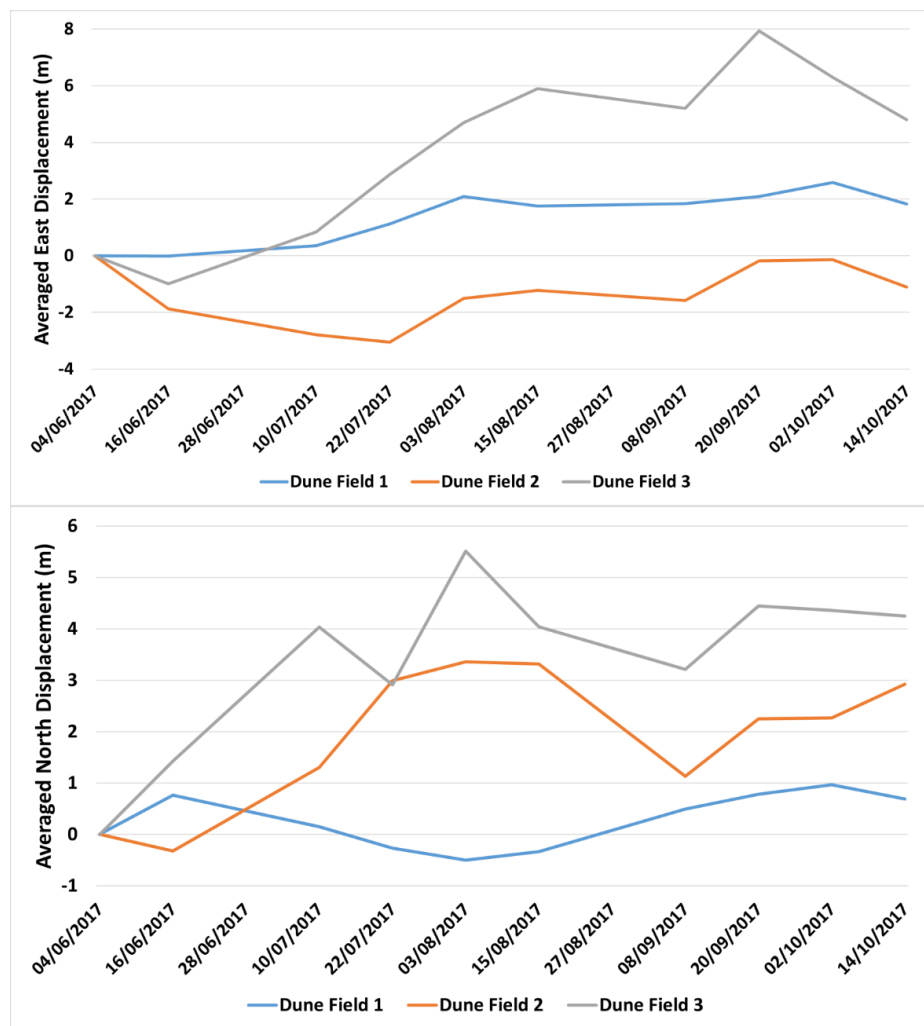


Figure 6. Spatially averaged east and north displacement time series with respect to the first SAR acquisition date (4 June 2017) for dune fields 1, 2 and 3.

The 0.62 ± 0.46 m threshold used to determine the movement of the dunes was proved to be reliable, as the GCPs in the built-up area are stable (Table 3).

Table 3. Displacements of the stable built up areas.

Date	Minimum Displacement (m)	Maximum Displacement (m)	Mean Displacement (m)	Standard Deviation (m)
4–16 June 2017	0.34	0.88	0.64	0.15
16 June–10 July 2017	0.32	0.98	0.64	0.20
10–22 July 2017	0.52	0.82	0.68	0.08
22 July–3 August 2017	0.73	1.20	0.94	0.13
3–15 August 2017	0.04	0.80	0.35	0.18
15 August–8 September 2017	0.23	0.89	0.54	0.18
8–20 September 2017	0.45	0.77	0.61	0.10
20 September–2 October 2017	0.20	0.60	0.37	0.10
2–14 October 2017	0.51	1.11	0.82	0.21

4.2. Impact of Wind Speed and Direction on Sand Dune Movement

Wind is the main factor in the movement of sand dunes in deserts [32]. In Sudan during the Autumn season (July–October), the wind tends to blow from the south [1]. The azimuth of the dominant wind blowing direction for dune fields 1, 2 and 3 during the studied period was 181, 185 and 187 degrees, with an average wind speed of 4.6 m/s, 4.84 m/s and 4.84 m/s, respectively. The southerly wind (Figure 7) resulted in an average displacement of 0.7 m in dune field 1 and 2.7 m in dune field 3, where both had a dominant movement to the north-east with an azimuth of 56° , while dune field 2 had an average displacement of 2.5 m to the north, with an azimuth of 346° (Figure S3).

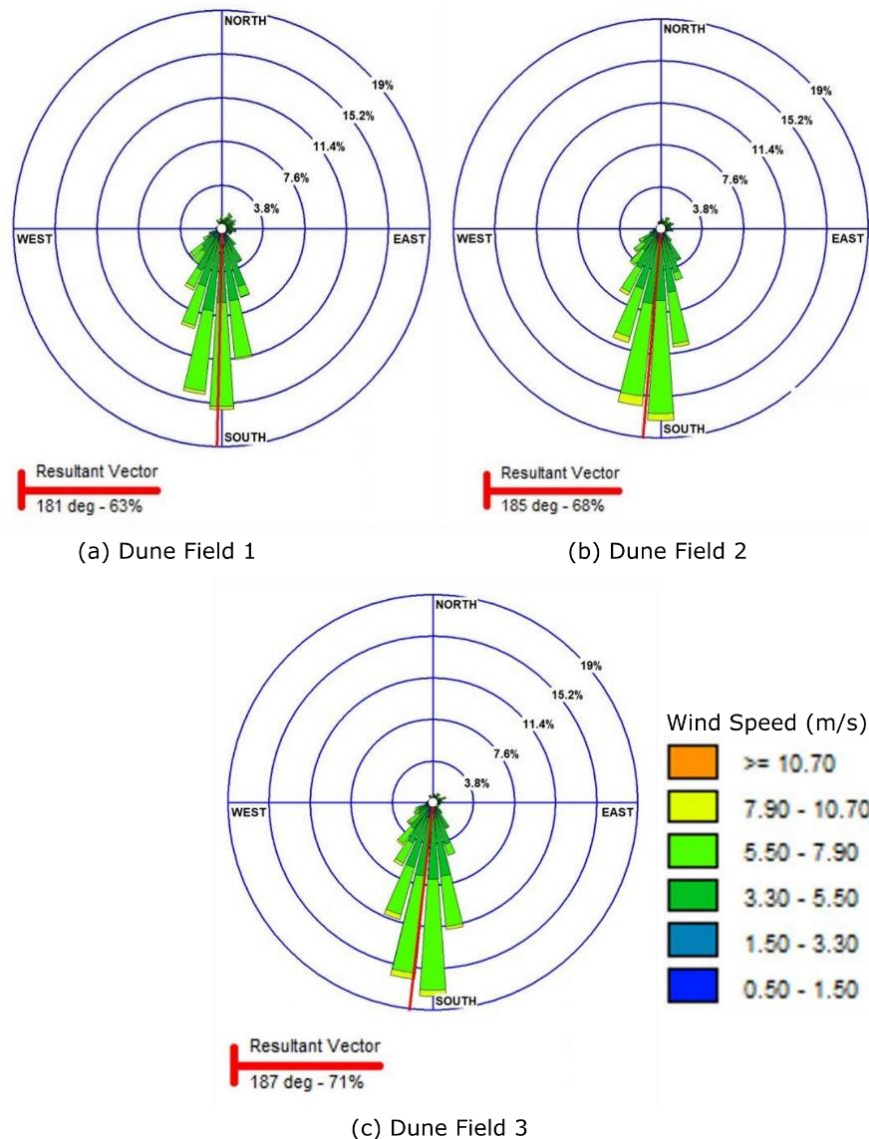


Figure 7. Wind rose maps of blowing wind for (a) dune field 1, (b) dune field 2, and (c) dune field 3.

The variation in wind components during the Autumn season resulted in drifting sand dunes in different directions. The sand dunes in dune field 1 moved in a consistent direction, and this was due to the impact of vegetation in controlling the movement (Figure 8), while the sand dunes in dune field 2 were divided into two groups according to their motion, which was probably a result of the mountainous topography that surrounds the dune field to the south and east sides (Figure 9). Dune field 3 had mostly consistent sand movement affected by its mountainous topography characteristics (Figure 10).

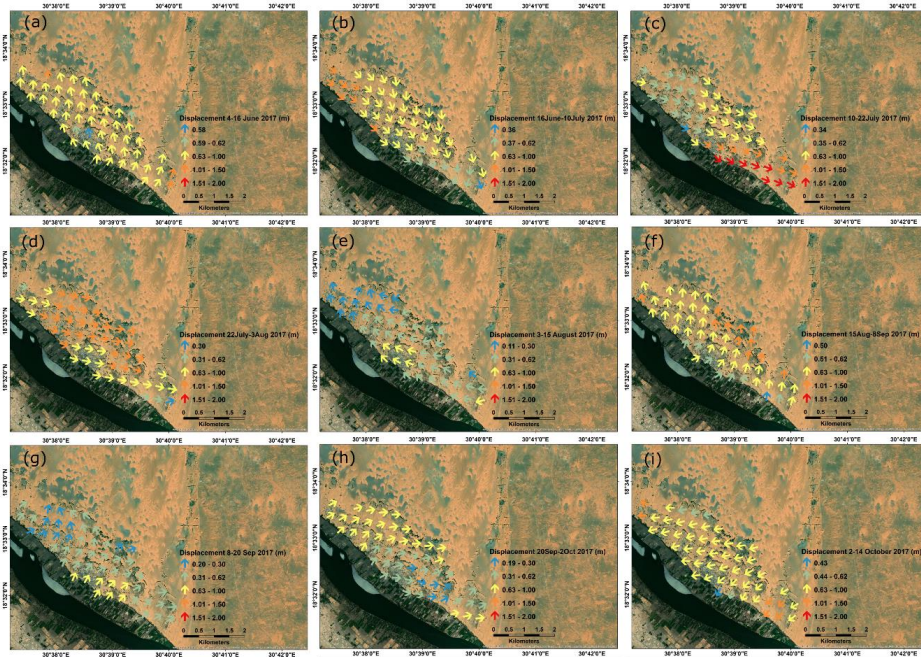


Figure 8. Displacement maps of dune field 1 for each pair of the SAR images. (a) Displacement map between 4 and 16 June 2017, (b) Displacement map between 16 June and 10 July 2017, (c) Displacement map between 10 and 22 July 2017, (d) Displacement map between 22 July and 3 August 2017, (e) Displacement Map between 3 and 15 August 2017, (f) Displacement map between 15 August and 8 September 2017, (g) Displacement map between 8 and 20 September 2017, (h) Displacement map between 20 September and 2 October 2017, (i) Displacement map between 2 and 14 October 2017.

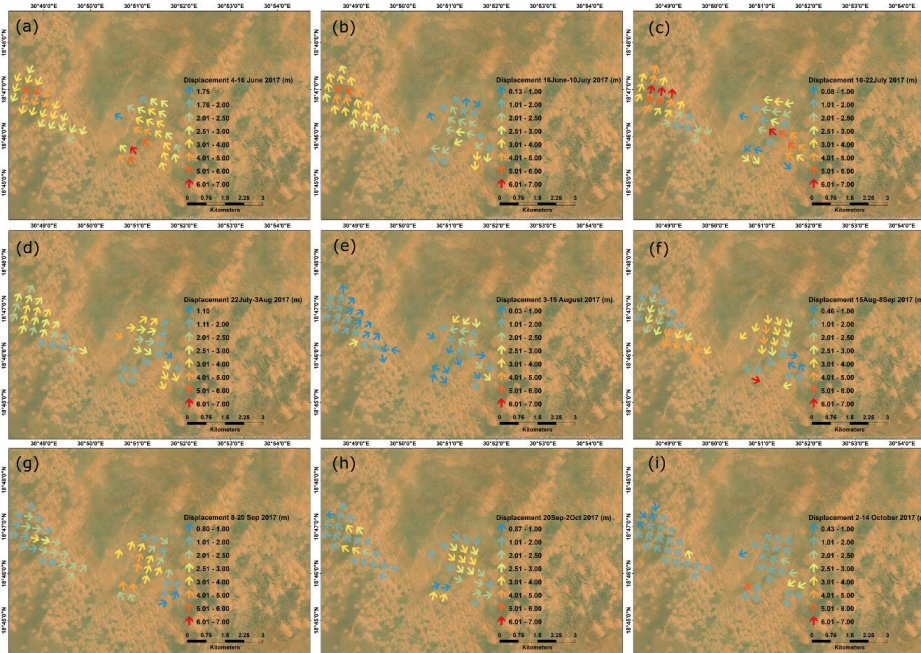


Figure 9. Displacement maps of dune field 2 for each pair of the SAR images. (a–i) are the sequence of displacement maps between 4 June to 14 October 2017.

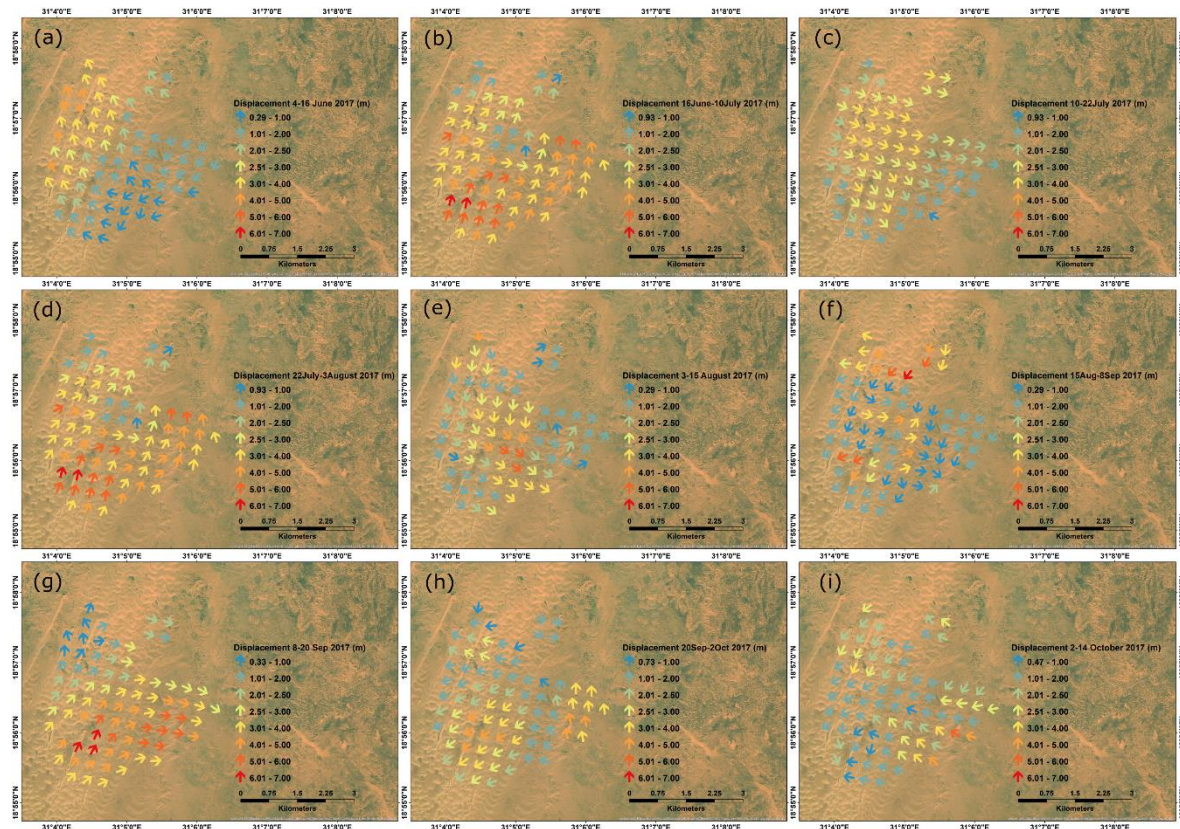


Figure 10. Displacement maps of dune field 3 for each pair of the SAR images. (a–i) are the sequence of displacement maps between 4 June to 14 October 2017.

4.3. Impact of Vegetation

A comparison was carried out to further determine the impact of vegetation cover on the movement of sand by considering the differences between the displacements of randomly selected dune points in the vegetated dune field 1 and the displacements of dune points in non-vegetated dune fields 2 and 3 (Figure 11). Large displacements were observed in the non-vegetated dune fields 2 and 3 with an average displacement of 2.4 and 2.6 m, respectively, compared to the average displacement of stable areas of 0.6 m, which is similar to the stability threshold of 0.62 ± 0.46 m determined for the built-up areas. Dunes in the vegetated dune field have a small average displacement of 0.7 m, similar to the stable area. This clearly shows the impact of vegetation in slowing down the movement of sand. This supports the recommendation of using vegetation for stabilizing dunes in agricultural and built up areas in Sudan [1].

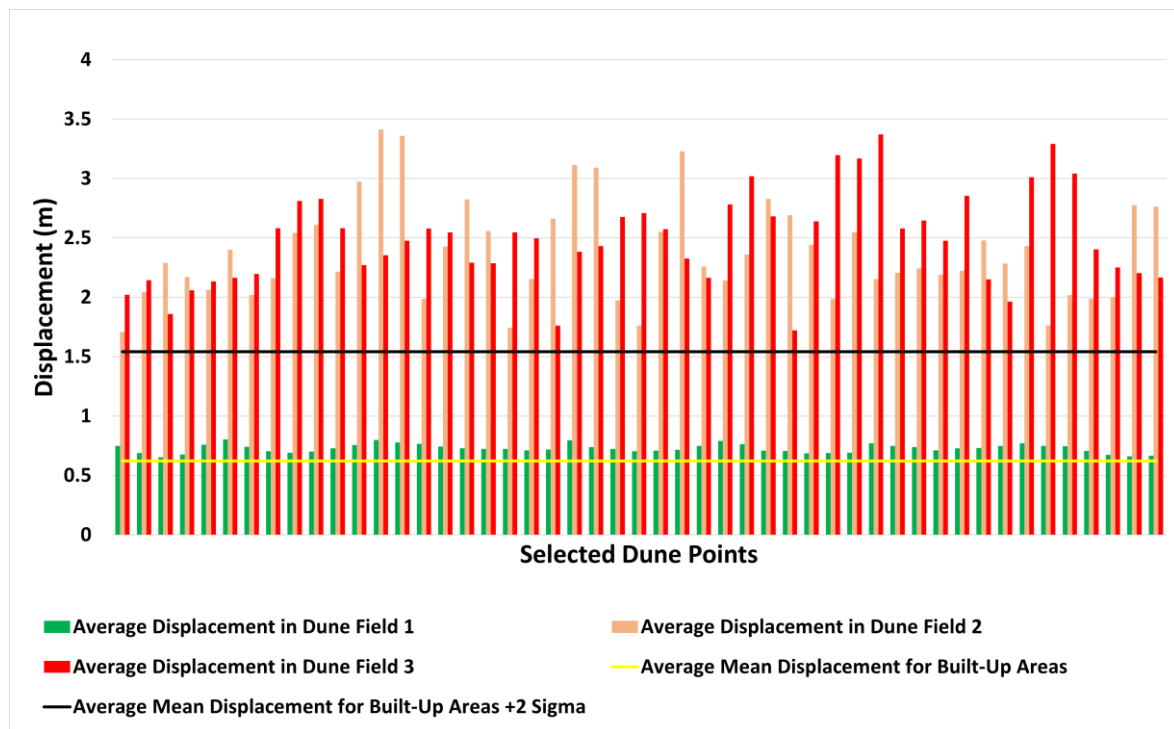


Figure 11. Average displacement of dune fields 1, 2 and 3 for randomly selected points compared to the stable zone of the built-up areas.

5. Discussion

5.1. Analysis of Dune Displacement

Wind blew mostly from the south, pushing the sand towards the north, which is to the opposite direction of its normal movement during the Spring and Summer seasons, i.e., to the south [1]. We discuss here some cases of the displacements of dune fields 1, 2 and 3 under normal and gusty wind conditions to show the impact of the variation in the influencing factors on the dune displacements.

The first case is under a normal wind condition, just before the start of the autumn season in Sudan, in the period between 4 to 16 June 2017 with a wind blowing dominantly from the south with an average wind speed of 4.9 m/s. This resulted in an average displacement of 0.8 m, 3.5 m and 1.9 m for dune fields 1, 2 and 3, respectively (Figure S1). Dune field 1 had movement direction towards the north north-east (Figure 8a) which reflects the impact of the dominant wind direction. The movement in dune field 2 had two dominant movement directions (Figure 9a); the east side of the dune field near the borders with the mountain had resulted in a diverted movement to the north-west, while the west side of the dune field moved in an opposite direction, to the south-west. This is most likely due to the impact of topography (Figure 2) forming a local counter-clockwise wind vortex, where the western arm of the vortex has wind motion towards the south. These types of localised wind phenomenon are not included in the more regional ERA5 wind models. Dune field 3 is surrounded with mountains from the south, east and west sides (Figure 2). This had an impact on its movement, which can be clearly seen in the diverted motion with a dominant component towards the north-west (Figure 10a).

The second case shows the displacement of the dunes in the period between 8 to 20 September with a wind blowing dominantly from the south with an average speed of 4.9 m/s. However, a northerly gusty wind with an average wind speed of 7.6 m/s occurred on 12 September. This resulted in an averaged displacement of 0.4 m, 2.4 m and 3.4 m for dune fields 1, 2 and 3, respectively (Figure S1). Dune field 1 had a movement direction towards the north-east (Figure 8g), which reflects the impact of the dominant wind direction but also shows that the vegetation cover impact in stabilising the

movement of the dunes and potentially preventing the impact of the easterly wind. Whereas the movement in dune field 2 had two dominant movement directions (Figure 9g); the east side group of dune points moved to the north while the west side group of the dune points moved to the east. This is most likely due to both the impact of the northerly gusty wind on 12 September and the impact of the of the strong westerly wind component, which exceeded the speed of 5.5 m/s during the period between 8 to 20 September (Figure 3). Regarding dune field 3, the dune points had a displacement to the north-east (Figure 10g) affected by the northerly gusty wind on 12 September and the impact of the westerly wind component during the period between 8 and 20 September.

The third case is the displacement of the dunes in dune field 1 between 16 June and 10 July to the south-east, even though the dominant wind direction for the period between 16 June and 28 June was blowing from the south. The two north-easterly gusty wind occurred between 20 to 22 June and between 4 and 5 July, which exceeded 9.5 m/s wind speed, resulted in this movement (Figure 8b). We have to mention here that the time interval between the two available SAR images for this offset image is 24 days, a larger temporal interval compared to the 12 days for the rest of the pairs. The north cumulative displacement continued moving south, reaching the maximum southward displacement in the period between 22 July and 3 August 2017 due to the occurrence of several northerly/north-easterly gusty winds. Afterwards, the dunes started to move gradually to the north (Figure S2a).

In general, the displacement time series for dune field 1 (Figure 6) show a larger movement in the east cumulative displacement compared to the northern component and this is due to the impact of the wall of trees in diverting the movement of the dunes parallel to its orientation. Dune field 2 had larger movement in the north component, while dune field 3 had the largest movement between the three dune fields in both east and north components.

A correlation analysis was carried out to identify the relationship between the displacement of the dunes and the wind by computing the Pearson correlation coefficient for dune fields 1, 2 and 3. In general, most of the correlations are positive, which shows that wind direction directly affects sand motion, apart from in dune field 1, which could be the impact of the tree line. Dune field 2 has poor correlation in the east, probably because of the two vortexes seen in the measurements caused by local topography, which are not picked up by the coarse wind measurements. The correlations are not perfect, because of the variability of the wind gusts and the timing difference between wind and dune measurements, Table 4, Figure S4.

Table 4. Pearson correlation analysis between the average east displacement and U wind and between average north displacement and V wind for dune fields 1, 2 and 3.

Dune Field	Pearson Correlation Coefficient (r)	
	E	N
Dune Field 1	0.42	−0.36
Dune Field 2	0.02	0.30
Dune Field 3	0.62	0.30

5.2. Reflection on Other Studies

Other studies have shown a clear correlation between the movement of sand dunes and the impact of wind, vegetation cover and topography. Munro et al. 2012 and Abuzid 2009, found that sand moves interchangeably in different directions and that during the Autumn season sand drifts to north as a result of the southerly wind [1,33]. Our study showed several variations in the direction of dune movement during the Autumn season; however, most of the displacement computed in this study showed a dominant movement to the north-east for dune fields 1 and 3, and a movement to the north for dune field 2 (Figure S3). This movement coincides with the dominant direction of the wind in the autumn season (southerly wind). Munro et al. 2012, showed similar sand drifting during the same season [1]. However, they also reported some southerly sand drifting cases that we clearly seen in our study as a result of the occurrence of several gusty wind episodes blowing from the north.

The impact of vegetation cover on sand dune motion has been reported in many studies, where it reduces the wind speed blown over the sand dunes [32]. Vegetation cover has been used to control the movement of dunes in deserts [1,34] and coastal areas and beaches [35,36]. Salih et al. 2017 stated that any increase in the vegetation cover results in more stability of the sand motion [37]. Additionally, Thomas and Tsoar 1990 stated that vegetation has a significant role in slowing down the movement of dunes and that sand dunes which migrate actively are less vegetated than those that migrate slowly [5]. Baoli and Tom 2015 conducted research on mapping sand dunes from satellite images; however, they excluded dune fields with the presence of vegetation cover, as they claimed that it was difficult to interpret the behaviour of the dunes due to the uncertainty resulting from vegetation [38]. However, in this research, the comparison between the vegetated dune field 1 with the non-vegetated dune fields 2 and 3 clearly showed the impact of vegetation cover in stabilizing the movement of the dunes. Additionally, it affected the dune points to the edge of the barrier wall of trees more in dune field 1, where most of the dunes were deviated in parallel, which visibly shows the impact of the vegetation.

Other studies have reflected on the impact of topography in the movement of the dunes [32]. Suliman 2012 showed in his study on sand dune movement in the north-west coastal region of Libya that the topography is the most important factor in shaping the dunes, while the sand particles are also diverted due to the mountainous topography [35], which we also saw clearly in our study.

As the detected movement by SAR offset tracking is the horizontal sand dunes movement, this raises an interesting question that should be firmly answered as to how to detect the impact of vertical sand dune motion and what the correlation is between the horizontal and vertical movement of sand dunes. Answering this will require further work and necessitate high-resolution digital elevation models.

5.3. Limitations

Despite the SAR pixel offset technique showing reliable and accurate results, we can highlight some limitations for the used images and wind data.

An important limitation to the use of SAR data to monitor sand dune motion in Sudan is the revisit frequency of the Sentinel-1 constellation. We attempt to minimise this by only using image pairs that have the smallest temporal (≤ 24 days) and spatial baselines (≤ 16 m). However, large displacements that occur within the satellite revisit time can still cause decorrelation and registration errors. The acquisition frequency for Sentinel-1 over Sudan is 12 days, which is not good enough to detect the impact of individual wind storms as the gusty winds tend to occur quite significantly during shorter periods (a few days at most) in the Autumn season [1] (Figure 3). This technique might work better for detecting coastal sand movement in Europe, where the temporal coverage of Sentinel-1 images is higher (every 6 days) compared to Sudan and Africa in general. A way to overcome this is by using high temporal resolution images acquired by other sensors (e.g., ALOS, TerraSAR-X, COSMO-Sky-Med and RadarSat-2 satellites) [39].

The ERA5 modelled wind data does not take into account the local high-resolution topography and trees, where its impact was seen in the different dune movement behaviours in the three dunes fields. This is considered a limitation of the ERA5 data. However, in this study, the DEM used for the analysis provided an understanding of the topography and its impact in diverting the movement of sand. The impact of rocky surfaces was reported by Bagnold 1941 [1], as in dune fields 2 and 3, where it resulted in higher saltation and led to larger movement, which reflects the impact of topography. Having ground recording weather stations would be the optimum solution to have accurate measurements of the wind data.

5.4. Regional Impact

Over the whole study period, large movements were detected in other areas that contain sand dunes, which indicates that sand moves faster than the other land features in the study area, with an average velocity ranging between 0.15 and 0.32 m/day, which was used to identify the most vulnerable

areas of sand movement in the region (Figure 12). Some agricultural projects, villages and part of the roads are affected by this large movement of sand. Therefore, the SAR offset tracking technique can provide a risk mapping technique, identifying the areas exposed to high degrees of sand drift.

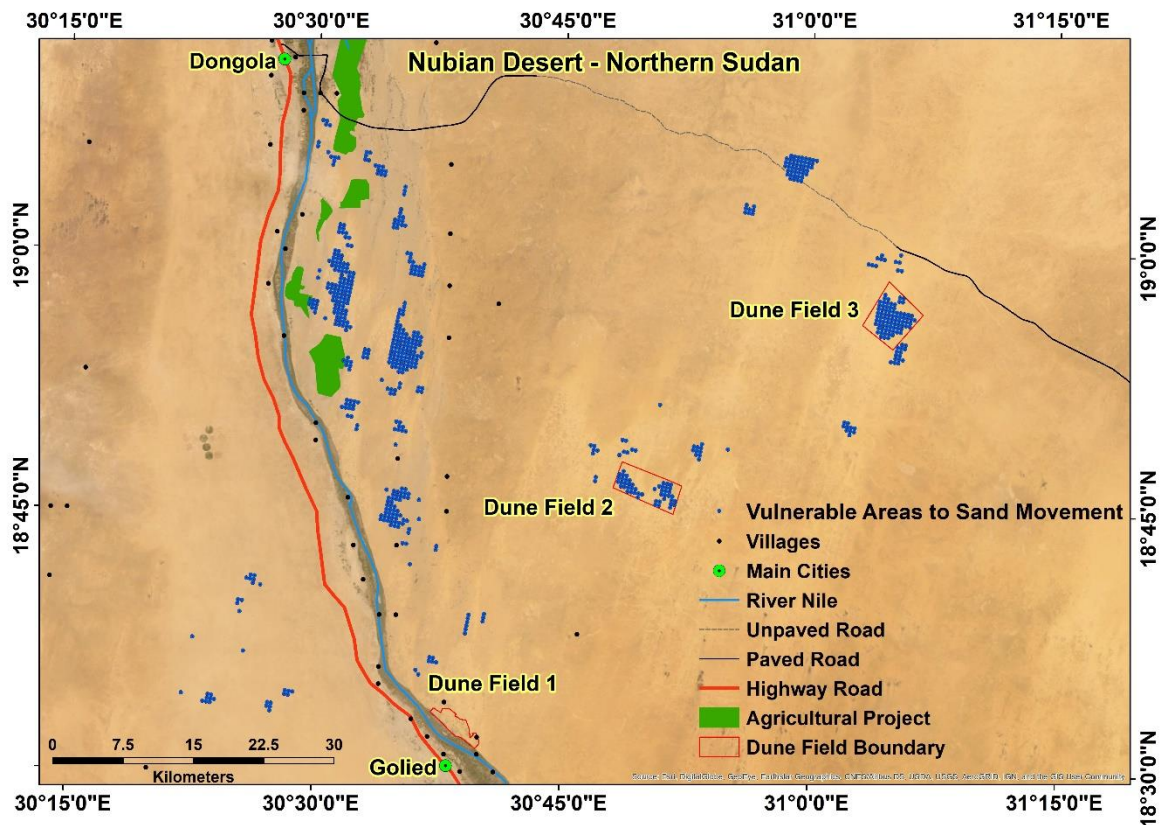


Figure 12. Vulnerable areas to sand movement.

6. Conclusions

This is the first application of SAR offset tracking in detecting the movement of sand dunes. In this research, the impacts of the influencing factors (wind speed/direction, vegetation and topography) on the dune movement were investigated. The cumulative east displacement over the four months study period was 1.8 m, -1.1 m and 4.8 m for dune fields 1, 2 and 3, respectively, while the cumulative north displacement was 0.7 m, 2.9 m and 4.2 m. It was found that the vegetation significantly slows down the movement of the dunes, with high displacements being observed in the non-vegetated dune fields 2 and 3, with an average displacement of 2.4 m and 2.6 m, respectively, over a study period of four months (4 June to 14 October 2017) compared to the average displacement of stable areas of 0.62 m. The vegetated dune field 1 had a small average displacement of 0.7 m, similar to the stable areas. The pixel offset results showed a positive correlation between the wind speed/direction and the dune movement. This impact of the wind cannot be separated from the impact of vegetation cover and topography; however, the impact of vegetation can be clearly observed when comparing the vegetated dune field 1 and the non-vegetated dune fields 2 and 3, while the impact of mountainous topography can be observed in dune field 2 and 3, diverting the direction of the movement, mainly near the edges of the mountains.

To achieve a better understanding of the movement of sand dunes, high temporal resolution imagery is required in order to detect the small movements that tend to happen on a daily basis. Additionally, the land cover characteristics of the dune field have a significant impact on the movement of the dunes; therefore, having high-resolution accurate DEMs will ensure better understanding of the impact of topography and vegetation cover on the sand dune movement.

This research identified areas with large sand dune movements that can be considered for further investigations and field works. The SAR offset tracking technique can play an important role in detecting and modelling sand movement by highly detailed monitoring of the sand dune fields. It can also support planning regional projects of combating desertification and sand movement.

Supplementary Materials: The following are available online at <http://www.mdpi.com/2072-4292/12/20/3410/s1>.

Author Contributions: Conceptualization, A.M.A.M., S.M., P.P., M.S.; methodology, A.M.A.M., A.N. and E.H.; software, A.M.A.M.; validation, A.M.A.M., A.N. and E.H.; formal analysis, A.M.A.M., A.N. and E.H.; investigation, A.M.A.M., A.N. and E.H.; resources, A.M.A.M.; data curation, A.M.A.M.; writing—original draft preparation, A.M.A.M.; writing—review and editing, A.M.A.M., A.N., E.H., S.M., P.P., M.S.; visualization, A.M.A.M.; supervision, S.M., P.P., M.S., A.N., E.H.; project administration, A.M.A.M. All authors have read and agreed to the published version of the manuscript.

Funding: This work was in part funded by the British Geological Survey University Funding Initiative (BUFI) PhD studentship (S448).

Acknowledgments: The authors would like to acknowledge the Copernicus Climate Change Service (C3S) for providing access to the ERA5 reanalysis data. Appreciation to the Lakes Environmental for providing access to the WRPLOT View software for plotting rose maps.

Conflicts of Interest: The authors declare no conflict of interest.

References

- Munro, R.; Ibrahim, M.A.M.; Abuzied, H.; el-Hassan, B. Aeolian sand landforms in parts of the Sudan and Nubia. Origins and impacts on past and present land use. Sudan & Nubia. *Sudan Archeol. Res. Soc.* **2012**, *16*, 140–154.
- Latif, M.A.A.; Elhag, M.M. Combating Desertification in Sudan. *Environment and Ecology at the Beginning of 21st Century*. 2015, p. 256. Available online: <https://www.researchgate.net/publication/291832376> (accessed on 6 September 2020).
- El Moghraby, A.I.; Ali, O.; el Seed, M.T. Desertification in Western Sudan and strategies for rehabilitation. *Environ. Conserv.* **1987**, *14*, 227–231. [[CrossRef](#)]
- Eljack, E.; Csaplovics, E.; Adam, H. Mapping and assessment of sand encroachment on the Nile River northern Sudan, by means of remote Sensing and GIS. In Proceedings of the Conference on International Research on Food Security, Natural Resource Management and Rural Development, Zurich, Switzerland, 14–16 September 2010.
- Lancaster, N. *Geomorphology of Desert Dunes*; Routledge: London, UK, 1995.
- Gómez, D.; Salvador, P.; Sanz, J.; Casanova, C.; Casanova, J.-L. Detecting areas vulnerable to sand encroachment using remote sensing and GIS techniques in Nouakchott, Mauritania. *Remote Sens.* **2018**, *10*, 1541.
- Pye, K.; Tsoar, H. *Aeolian Sand and Sand Dunes*; Springer Science & Business Media: Heidelberg/Berlin, Germany, 2008.
- Zhou, X.; Chang, N.-B.; Li, S. Applications of SAR interferometry in earth and environmental science research. *Sensors* **2009**, *9*, 1876–1912. [[CrossRef](#)] [[PubMed](#)]
- Balzter, H.; Rowland, C.S.; Saich, P. Forest canopy height and carbon estimation at Monks Wood National Nature Reserve, UK, using dual-wavelength SAR interferometry. *Remote Sens. Environ.* **2007**, *108*, 224–239. [[CrossRef](#)]
- Tosi, L.; Strozzi, T.; Da Lio, C.; Teatini, P. Regional and local land subsidence at the Venice coastland by TERRASAR-X PSI. In *NISOLS 2015 (Ninth Symposium on Land Subsidence)*; Copernicus Publications: Göttingen, Germany, 2015.
- Massonnet, D.; Feigl, K.L. Radar interferometry and its application to changes in the Earth's surface. *Rev. Geophys.* **1998**, *36*, 441–500. [[CrossRef](#)]
- Pedersen, R.; Sigmundsson, F. Temporal development of the 1999 intrusive episode in the Eyjafjallajökull volcano, Iceland, derived from InSAR images. *Bull. Volcanol.* **2006**, *68*, 377–393. [[CrossRef](#)]
- Cai, J.; Wang, C.; Mao, X.; Wang, Q. An adaptive offset tracking method with SAR images for landslide displacement monitoring. *Remote Sens.* **2017**, *9*, 830. [[CrossRef](#)]

14. Refice, A.; Capolongo, D.; Pasquariello, G.; Addabbo, A.; Bovenga, F.; Nutricato, R.; Lovergine, F.P.; Piatrenera, L. SAR and InSAR for flood monitoring: Examples with COSMO-SkyMed data. *IEEE J. Sel. Top. Appl. Earth Observ. Rem. Sens.* **2014**, *7*, 2711–2722. [[CrossRef](#)]
15. Blumberg, D.G. Remote sensing of desert dune forms by polarimetric synthetic aperture radar (SAR). *Remote Sens. Environ.* **1998**, *65*, 204–216. [[CrossRef](#)]
16. Maghsoudi, M.; Hajizadeh, A.; Nezammahalleh, M.A.; Seyedrezai, H.; Jalali, A.; Mahzoun, M. Interferometric Synthetic aperture radar (INSAR) technology and geomorphology interpretation. *ISPRS Int. Arch. Photogramm. Remote Sens. Spat. Inf. Sci.* **2013**, 253–256. [[CrossRef](#)]
17. Chang, X.; Guo, J.; Wang, X. Detecting the amount of eroded and deposited sand using DInSAR. *Terr. Atmos. Ocean. Sci.* **2011**, *22*, 187–194. [[CrossRef](#)]
18. Havivi, S.; Amir, D.; Schwartzman, I.; August, Y.; Maman, S.; Rotman, S.R.; Blumberg, D.G. Mapping dune dynamics by InSAR coherence. *Earth Surf. Process Landf.* **2018**, *43*, 1229–1240. [[CrossRef](#)]
19. Casu, F.; Manconi, A.; Pepe, A.; Lanari, R. Deformation time-series generation in areas characterized by large displacement dynamics: The SAR amplitude pixel-offset SBAS technique. *IEEE Trans. Geosci. Remote Sens.* **2011**, *49*, 2752–2763. [[CrossRef](#)]
20. Riveros, N.; Euillades, L.; Moreiras, S.; Balbarani, S. Offset tracking procedure applied to high resolution SAR data on Viedma Glacier, Patagonian Andes, Argentina. *Adv. Geosci.* **2013**, *35*, 7–13. [[CrossRef](#)]
21. Pepe, A.; Caló, F. A review of interferometric synthetic aperture RADAR (InSAR) multi-track approaches for the retrieval of Earth's surface displacements. *Appl. Sci.* **2017**, *7*, 1264. [[CrossRef](#)]
22. Strozzi, T.; Luckman, A.; Murray, T.; Wegmuller, U.; Werner, C.L. Glacier motion estimation using SAR offset-tracking procedures. *IEEE Trans. Geosci. Remote Sens.* **2002**, *40*, 2384–2391. [[CrossRef](#)]
23. Wang, T.; Wei, S.; Jónsson, S. Coseismic displacements from SAR image offsets between different satellite sensors: Application to the 2001 Bhuj (India) earthquake. *Geophys. Res. Lett.* **2015**, *42*, 7022–7030. [[CrossRef](#)]
24. Wang, T.; Jónsson, S. Improved SAR amplitude image offset measurements for deriving three-dimensional coseismic displacements. *IEEE J. Sel. Top. Appl. Earth Obs. Remote Sens.* **2015**, *8*, 1–8. [[CrossRef](#)]
25. Ou, D.; Tan, K.; Du, Q.; Chen, Y.; Ding, J. Decision fusion of D-InSAR and pixel offset tracking for coal mining deformation monitoring. *Remote. Sens.* **2018**, *10*, 1055. [[CrossRef](#)]
26. Ayoub, F.; Avouac, J.-P.; Newman, C.; Richardson, M.; Lucas, A.; Leprince, S.; Bridges, N. Threshold for sand mobility on Mars calibrated from seasonal variations of sand flux. *Nat. Commun.* **2014**, *5*, 5096. [[CrossRef](#)]
27. Thomas, N.; Nigam, S. Twentieth-century climate change over Africa: Seasonal hydroclimate trends and Sahara desert expansion. *J. Clim.* **2018**, *31*, 3349–3370. [[CrossRef](#)]
28. NASA. Dust Storm over Sudan and the Red Sea. Available online: https://modis.gsfc.nasa.gov/gallery/individual.php?db_date=2017-08-17 (accessed on 6 December 2019).
29. Dee, D.P.; Uppala, S.M.; Simmons, A.J.; Berrisford, P.; Poli, P.; Kobayashi, S.; Andrae, U.; Balmaseda, M.A.; Balsamo, G.; Bauer, P.; et al. The ERA-Interim reanalysis: Configuration and performance of the data assimilation system. *Q. J. R. Meteorol. Soc.* **2011**, *137*, 553–597. [[CrossRef](#)]
30. Copernicus Climate Change Service Climate Data Store (CDS). ERA5: Fifth Generation of ECMWF Atmospheric Reanalyses of the Global Climate. Available online: <https://cds.climate.copernicus.eu/cdsapp#!/software/app-era5-explorer?tab=overview> (accessed on 6 December 2019).
31. Hoffmann, L.; Günther, G.; Li, D.; Stein, O.; Wu, X.; Griessbach, S.; Heng, Y.; Konopka, P.; Müller, R.; Vogel, B.; et al. From ERA-Interim to ERA5: The considerable impact of ECMWF's next-generation reanalysis on Lagrangian transport simulations. *Atmos. Chem. Phys. Discuss.* **2019**, *19*, 3097–3124. [[CrossRef](#)]
32. Kok, J.F.; Parteli, E.J.R.; Michaels, T.; Karam, D.B. The physics of wind-blown sand and dust. *Rep. Prog. Phys.* **2012**, *75*, 106901. [[CrossRef](#)] [[PubMed](#)]
33. Abuzied, H. Mapping and Assessment of Wind Erosion in Central Northern State, Sudan. Ph.D. Thesis, Desertification and Desert Cultivation Studies Institute, University of Khartoum, Khartoum, Sudan, 2009.
34. Berte, C.J. *Fighting Sand Encroachment: Lessons from Mauritania*; Food and Agriculture Organization of the United Nations (FAO): Rome, Italy, 2010.
35. Koja, S.F. *Sand Dune Movement and its Impact on Human Activities in the North Western Coast Region of Libya. An Analysis of the Sediment Characteristics of Sand Dunes, and Their Movement Using Satellite Images, and the Effects of Encroachment on Farms Assessed by a Questionnaire Survey*; University of Bradford: Bradford, UK, 2012.
36. Durán, O.; Moore, L.J. Vegetation controls on the maximum size of coastal dunes. *Proc. Natl. Acad. Sci. USA* **2013**, *110*, 17217–17222. [[CrossRef](#)] [[PubMed](#)]

37. Salih, A.A.; Ganawa, E.-T.; Elmahl, A.A. Spectral mixture analysis (SMA) and change vector analysis (CVA) methods for monitoring and mapping land degradation/desertification in arid and semiarid areas (Sudan), using Landsat imagery. *Egypt. J. Rem. Sens. Space Sci.* **2017**, *20*, S21–S29. [[CrossRef](#)]
38. Liu, B.; Coulthard, T.J. Mapping the interactions between rivers and sand dunes: Implications for fluvial and aeolian geomorphology. *Geomorphology* **2015**, *231*, 246–257. [[CrossRef](#)]
39. Fallourd, R.; Harant, O.; Trouve, O.; Nicolas, J.-M.; Gay, M.; Walpersdorf, A.; Mugnier, J.-L.; Serafini, J.; Rosu, D.; Bombrun, L.; et al. Monitoring temperate glacier displacement by multi-temporal TerraSAR-X images and continuous GPS measurements. *IEEE J. Sel. Top. Appl. Earth Obs. Remote Sens.* **2011**, *4*, 372–386. [[CrossRef](#)]

Publisher's Note: MDPI stays neutral with regard to jurisdictional claims in published maps and institutional affiliations.



© 2020 by the authors. Licensee MDPI, Basel, Switzerland. This article is an open access article distributed under the terms and conditions of the Creative Commons Attribution (CC BY) license (<http://creativecommons.org/licenses/by/4.0/>).